Asian Journal of Chemistry; Vol. 36, No. 8 (2024), 1921-1926

ASIAN JOURNAL OF CHEMISTRY

https://doi.org/10.14233/ajchem.2024.31255

Synthesis of Zinc-based Bimetallic Nanoparticles for the Degradation of Industrial Dyes

N. SRIVASTAVA and K. RAEES*

Department of Chemistry, University Institute of Sciences, Chandigarh University, Mohali-140413, India

*Corresponding author: E-mail: raeeskashif@gmail.com

Received: 16 January 2024; *Accepted*: 8 July 2024; *Published online*: 25 July 2024; AJC-21714

Textile dyes are a prominent source of coloured organic substances that present an increasingly concerning risk to biodiversity. This problem could be remediated by incorporating nanoparticles as photocatalysts in photodegradation activities. The photocatalytic degradation of brilliant blue and Amaranth dyes has been investigated using ZnO-Fe_2O_3 bimetallic nanoparticles (Zn-Fe BN) in an aqueous media under sun rays. The Zn-Fe BN was synthesized using a chemical synthesis technique utilizing $FeCl_3$ and $ZnSO_4 \cdot 7H_2O$ as starting materials and further characterized using XRD, FTIR, SEM, EDAX and DLS techniques. The degradation rate was examined by recording the absorbance value *via* a UV-Vis spectrophotometer. The experimental results demonstrated that the synthesized Zn-Fe BN was an effective catalyst in removing the dyes from water. The decomposition rate was effective with variations in the reaction parameters. As the concentration of the NaOH solution was increased, an increment in the rate of degradation was observed simultaneously, as well as for different amounts of catalyst. Hence, the removal of textile dyes could be made easier by adopting the methodology.

Keywords: Bimetallic nanoparticles, Zinc-based nanoparticles, Dye degradation, Photocatalysis, Industrial dyes.

INTRODUCTION

In India, the textile industry is a significant and swiftly developing industrial sector. The textile business makes use of a variety of resources, including cotton, wool and synthetic fibers. A large amount of industrial waste is generated from the apparel business, remarkably an eminent industry [1]. Given a higher demand for water for its various wet-treatment techniques, the textile sector is a major contributor to effluent wastewater production. As a result, the textile sector is thought to have the greatest worldwide demand for water and the highest level of pollution in its wastewater discharges of any business. Water usage in textile mills on an average size is approximately 200 L/Kg of cloth manufactured daily [2]. Contaminants like acids, alkalis, hydrogen peroxide, colloids, dispersants and metal constituted cleaners exist ineffluent wastes [3].

Approximately 60-70% of azo dyes are toxic, carcinogenic and resistant to physio-chemical treatments. Following their molecules breakdown and the formation of aromatic amines like benzidine, dimethoxy-benzidine and dimethyl-benzidine, azo dyes become toxic [4,5]. By electrostatically adhering to sediments or drainage sludge, azo ionic dyes that are dumped on the ground or sewerage may attach to suspended organic materials, prolonging their permanence [6]. Furthermore, coloured water or polluted sludge that comes into touch with marine life spreads harmful chemicals to mankind as well *via* the food chain leading to ailments such as cramps, elevated blood pressure, vomiting, hemorrhage and blistering of the skin. Significant harm to the renal system, reproductive system, central nervous system and organs such as the liver and brain may result depending on the dye exposure dosages [7,8].

Conventional methods like filtration, chlorination and ozonation have shortcomings of particular importance, including the need for complementary energy sources and the creation of hazardous waste. Because of their potent oxidation capacities, affordability, eco-friendliness, photocatalytic degradation strategies of organic dyes ought to be appealing for the remediation of textile contaminants [9,10]. An innovative and successful technique for treating dye house discharge is semiconductor photocatalysis, which can dissolve pigment molecules into smaller components like CO_2 and water and neutralize them. This reduces the possibility of generating sludge and harmful byproducts, which frequently lead to additional challenges with treatment and disposal [11].

The problem could be remediated by incorporating nanoparticles, particularly bimetallic nanoparticles. The superior electrocatalytic performance and faster reaction time of bimetallic nanoparticles have led to their widespread application in electrochemical monitoring [12]. Bimetallic catalysts also show promising prospects for nitrate reduction applications from wastewater [13,14]. Furthermore, the Zn-based bimetallic nanoparticles play a significant role as a photocatalyst in photodegradation activities. Zinc oxide (ZnO) exhibits a high degree of mineralization and reactivity, making it a more effective catalyst for water purification. It also contains a greater quantity of highly reactive active sites on its surface [15], based on the higher starting activity rates and its efficiency in absorbing solar radiation [16]. With a large direct band gap energy (E_{bg} = 3.2 eV), ZnO is regarded as the second most popular photocatalyst. Remarkable photoreduction efficiency, antifouling and antibacterial qualities are displayed by ZnO. It exhibits superior photocatalytic effectiveness due to its increased electron mobility (200-300 cm^2/Vs), which enhances its quantum efficiency [17]. Improved photoinduced activity *via* enhanced light absorption rate and more accurate inhibition of photoinduced electron-hole pair recombination, thus preserving elevated charge separation, have been two primary advantages of associating two semiconductor metal oxides [18,19]. Moreover, nanoparticles having an amalgamated Fe-Zn crystalline matrix can be magnetically recovered, making them attractive for industrial usage due to the atomic structure of iron [20]. In addition, due to their distinctive chemical composition, compact dimensions, magnetic properties, organization and synergistic effects, such nanoparticles have the potential to be more efficient in their primary use and can be easily recovered or recycled. Therefore, Zn-Fe BN is considered as suitable for the photodegradation processes, to improve the environmental impacts caused by the dyestuff. For the purpose of adsorptive removal of the carcinogenic dyes brilliant blue and Amaranth from water, a new bimetallic Fe-Zn nanoparticle as photocatalyst was synthesized *via* a microwave irradiation.

EXPERIMENTAL

Ferric chloride anhydrous (96%; Nice Chemicals Pvt. Ltd., India), zinc sulphate heptahydrate (99%; Loba Chemie Pvt. Ltd., India), sodium hydroxide pellets (97%; Molychem, India), sodium dodecyl sulphate (99%; CDH, India). The brilliant blue (BB) (50%; Sigma-Aldrich) and Amaranth (AM) (85-95%; Sigma-Aldrich) were used as model dyes in this work. All the chemicals and reagents used were of analytical grade.

Synthesis of photocatalyst: The bimetallic nanoparticles used in the present study were synthesized under microwave irradiation. $FeCl_3$ (8 g) and $ZnSO_4 \cdot 7H_2O$ (14 g) were dissolved in distilled water by stirring vigorously for 15 min while heating at 80 ºC. Sodium dodecyl sulphate (SDS, 0.05 g) was added to the solution mixture acting as a stabilizing agent while stirring for further 15 min and the solution was agitated in a microwave reactor at 180 ºC for 30 min. Later, added 2 M of NaOH and NH_3 solutions dropwise to the above solution and again microwave irradiated at 180 ºC for 1 h. The deposition acquired was percolated, cleaned with distilled water followed by acetone and then dried for 6-7 h at 70 ºC in a hot air oven.

Characterization: The synthesized bimetallic nanoparticles were characterized by XRD using a MiniFlex II X-ray diffractometer from Rigaku, Japan, having a radiation source of Cu*K*α with λ = 1.4406 nm. FTIR spectrometer 'Nicolet iS50' from Thermo-Fisher Scientific, Madison, USA was used to record the FTIR data. Carl Zeiss Model Spra 55 was used for capture the SEM images and elements within the sample were observed with EDAX analysis using EDS, TESCAN-1105 instrument. The Zetasizer nano ZS, UK was used to record the DLS evaluation. A Shimadzu UV-1900 UV-Vis spectrophotometer from Kyoto, Japan was used to record the rate of photodegradation.

Kinetic measurements: All the kinetic assessments were conducted spectrophotometrically by working on a double-beam UV-Vis spectrophotometer. A 3 mL quartz cuvette having a 10 mm path length was employed to analyze the absorbance of the prepared samples at room temperature. The kinetic runs were carried out under the pseudo-first-order reaction conditions in which the concentration of NaOH was kept more than the quantity of other components in the reaction medium. The decrease in absorbance as a function of time was measured at a fixed wavelength for the selected dyes to monitor the degradation of the dyes.

A 100 mL volumetric flask was used to generate a working concentration (5×10^{-5} mol dm^{-3}) from stock solutions of brilliant blue (1×10^{-3} mol dm^{-3}) and Amaranth (1×10^{-3} mol dm^{-3}), which were dissolved in distilled water. The stock solutions of sodium hydroxide were prepared with different concentrations to investigate the effect of NaOH on the studied dyes. The requisite amounts of reactants (distilled water and respective dye) were taken in two separate 100 mL conical flasks. The zero-time absorbance was noted to attain the maximum absorbance for both dyes. The Amaranth dye shows its maximum absorption at λ_{max} = 521 nm while the brilliant blue dye demonstrates at λ_{max} = 556 nm. The reaction was then allowed to react with the desired amount of NaOH solution along with the synthesized Zn-Fe BN (0.005 g) in the reaction vessels. The reaction mixtures were kept under the natural sunlight and absorbance was recorded after the intervals of 15 min using the UV-Vis spectrophotometer and the rate constant was calculated from the slope of the plot of absorbance *versus* time. Similarly, the experiments were conducted with the desired amount of Zn-Fe BN in the reaction vessel with NaOH (0.1 mol dm^{-3}). Sunlight-assisted degradation was conducted and the absorbance was recorded after every 15 min of intervals. From June through August, solar exposure was executed on beaming sunny days from 9:00 am to 5:00 pm. Initally, the reaction happened quite quickly and the maximum degradation was discerned within 15 min of collision time.

RESULTS AND DISCUSSION

XRD studies: Fig. 1 shows the phase and structure size of the synthesized nanoparticles for characteristic reflections corresponding to a crystalline layered phase through XRD impression. The report of the nanoparticles exhibited peaks

related to Fe_2O_3 along with reflections of ZnO, which suggest the confirmed formation of Zn-Fe BN. The characteristic diffraction peaks of Fe_2O_3were observed at 2θ = 15.508º, 17.402º, 24.298º, 28.599º, 49.713º, 54.743º and 59.857º that correspond to the (110), (111), (012), (220), (024), (430) and (520) crystallographic planes, respectively. The lattice parameters for Fe_2O_3 matched well with the JCPDS no: 39-1346 and 33-0664. On the other hand, the diffraction spectrum at 2θ = 28.937º, 39.306º and 45.694º attributed to (100), (101) and (102) crystallographic planes, respectively were assigned to ZnO, which matched with JCPDS card no: 01-089-0510. The highest peaks are observed at 2θ = 28.599º and 28.937º for Fe_2O_3 and ZnO, respectively. These results confirmed the formation of Zn-Fe BN with high crystalline quality.

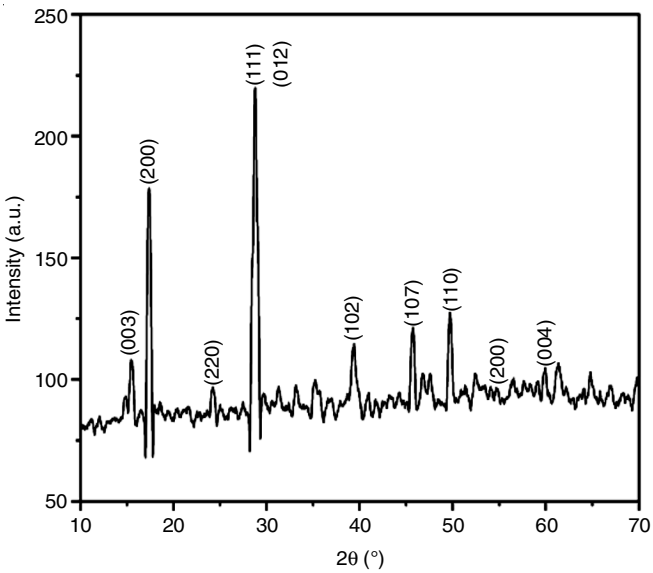

Fig. 1. X-ray diffraction spectrum of Zn-Fe bimetallic nanoparticles

FTIR studies: Fig. 2 shows the FTIR spectrum at room temperature which have approximate similarity to that reported in the literature [21,22]. In the FTIR spectrum of Zn-Fe BN, the broad strong adsorption band centered at 3307 cm^{-1} is attributed to O-H stretching vibration originating from the hydroxyl group, which is probably on account ofthe adsorption of water molecules on the top of nanoparticles. The peak at 2092 cm^{-1} is allotted to the -CH bands vibration of the -CH_2 group in SDS. A weaker band at 1624 cm^{-1} was given to the bending vibration mode of water molecules. The -CH_2 groups bending vibrations in SDS are localized at 1421 cm^{-1}. The peaks appearing at 1174 cm^{-1}, 1076 cm^{-1}, 983 cm^{-1} and 618 cm^{-1} corresponds to vibrations of S=O, whereas the peak 451 cm^{-1} is identified as the Fe-O bond.

SEM studies: Fig. 3 shows the SEM images of the synthesized Fe-Zn BN photocatalytic material. The nano-sized cubic sample appears to be in clusters with smooth surfaces at low magnification (Fig. 3a-b). Fig. 3c demonstrates the image at a higher magnification that indicates the interconnected cubic assembly from a nano-cluster shape. According to the results obtained from SEM, Zn-Fe BN has a size in the nanometer scale with cubic morphology.

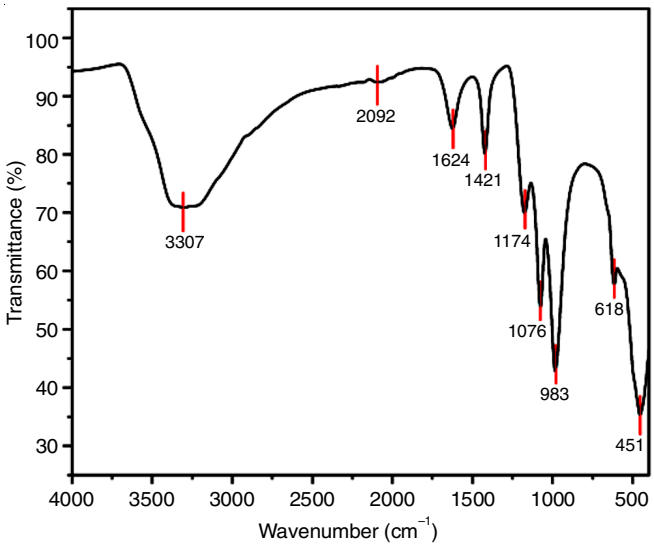

Fig. 2 FTIR spectra of synthesized Zn-Fe bimetallic nanoparticles

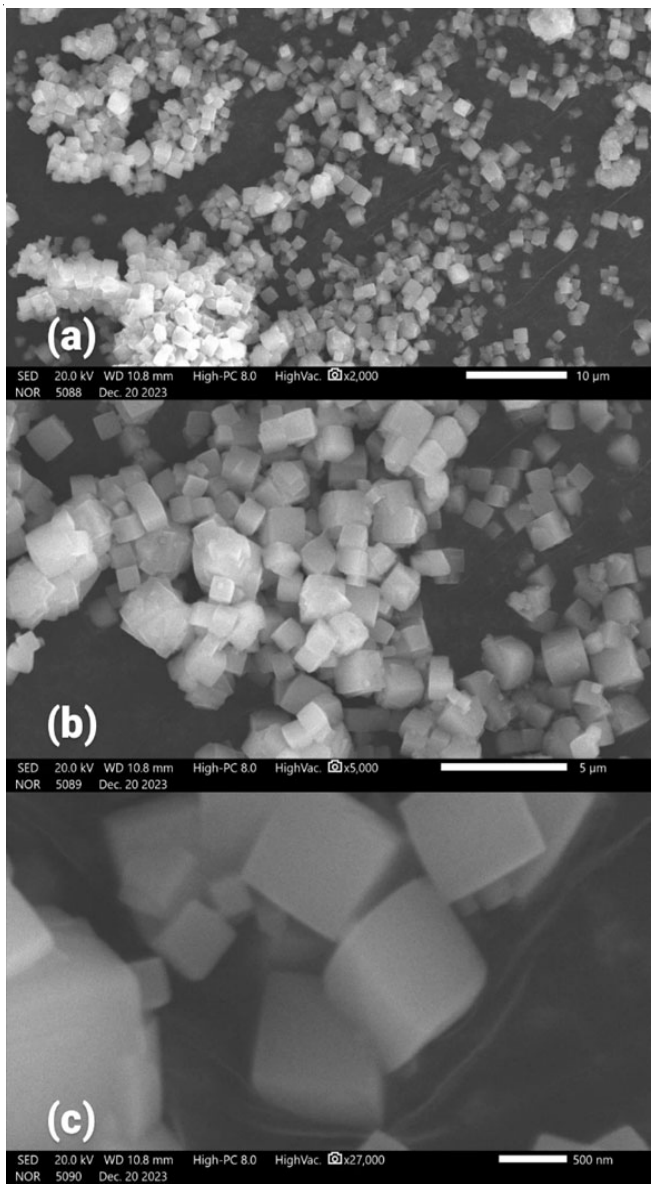

Fig. 3. SEM images of the synthesized Fe-Zn bimetallic nanoparticles

EDAX studies: Fig. 4 shows the chemical composition confirmed the presence of Zn and Fe in Zn-Fe bimetallic nanoparticles photocatalytic material. The elemental distribution of bimetallic Zn-Fe bimetallic nanoparticles exhibits 38.81% of zinc, 38.19% of iron and 23% of oxygen.

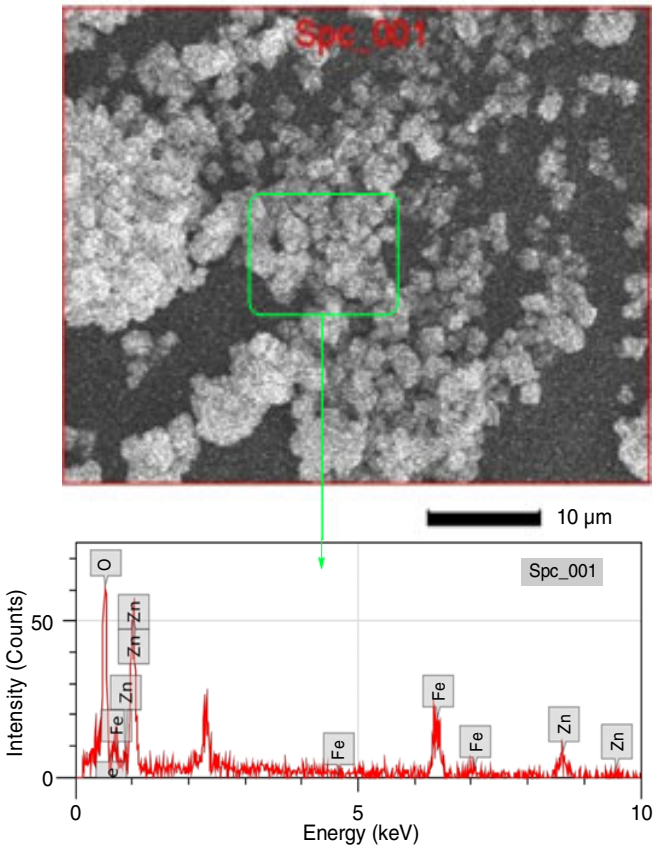

Fig. 4. EDAX spectrum of Zn-Fe bimetallic nanoparticles

Dynamic light scattering (DLS): Information on the size distribution can be found in the light scattered by the particles. DLS analyzed the particle size distribution is given in Fig. 5.

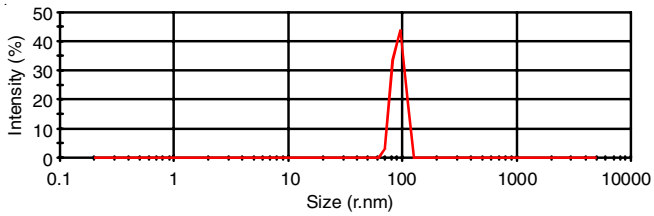

Fig. 5. DLS size distribution of Zn-Fe bimetallic nanoparticles

Degradation rate: The photocatalytic activity of the prepared bimetallic Zn-Fe BN photocatalyst was used to disintegrate brillant blue and Amaranth dyes under the influence of sunlight irradiation. The concentration of both dyes reduced as the period of sunshine exposure increased, ultimately showing that the photodecomposition of both dyes occurred in the presence of Zn-Fe BN. The degree of degradation of brillant blue was significantly faster in comparison to the moderate deterioration of Amaranth dye.

Influence of amount of Zn-Fe BN on degradation of dyes: Catalyst concentration significantly affects the degradation of both dyes (Fig. 6). Dye concentration was kept constant at 5×10^{-5} mol dm^{-3} and the evaluation of Zn-Fe BN effect on the degradation of brillant blue and Amaranth dyes was studied in the range between 0.005 g to 0.025 g. An increment in the amount of Zn-Fe BN showed an increment in the degradation rate. The maximum degradation was observed for 0.025 g of catalytic dose for Zn-Fe BN. Dye degradation increases with a rise in catalytic concentration till the saturation point, as is evident from the decrease in the rate of absorbance intensities with time. However, after the saturation point, the degradation decreases with the increase in the amount of catalyst. Dye degradation is proportional to the amount absorbed on the surface of the catalyst till the attainment of the saturation point. As per the available literature, the maximum quantity of solid catalyst used for the maximum degradation is 3-4 g/L of dye solution [23].

Influence of concentration of NaOH on the degradation of dyes: The reaction mixture was subjected to regular exami-

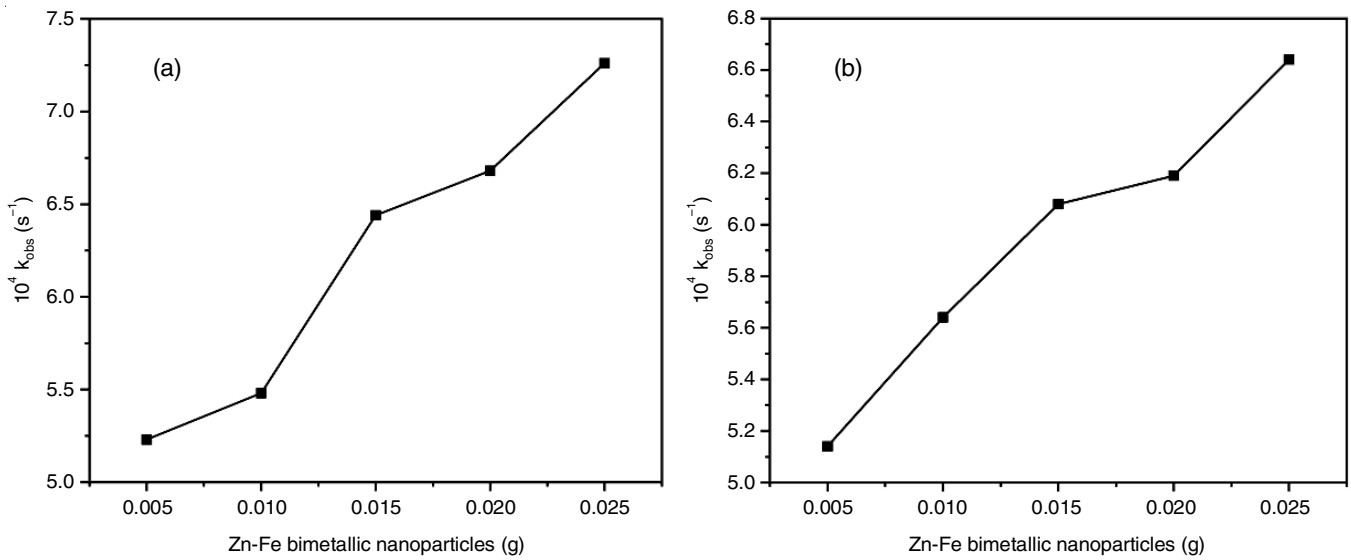

Fig. 6. Plots of rate constant *versus* varying amounts of Zn-Fe bimetallic nanoparticles for brilliant blue (a) and Amaranth (b)

nations at fixed time intervals of 15 min. These spectra indicated that the absorbance intensities at λ_{max} = 556 nm (brillant blue) and λ_{max} = 521 nm (Amaranth) progressively decreased with time. A decrease in the absorbance intensities was due to the degradation of the dyes due to the effect of NaOH concentration as well as the photocatalyst. To assess the effect of NaOH, the degradation rate of brilliant blue and Amaranth dyes was studied in the range of 2×10^{-3} mol dm^{-3} to 1×10^{-1} mol dm^{-3} concentrations. The observed results are presented in Fig. 7. The rate constant *versus* [NaOH] plot demonstrates that the value of the rate constant rises with advancements in the [NaOH], attributing that the degradation rate of brilliant blue and Amaranth dyes increases.

Comparative studies: The efficiency of the synthesized Zn-Fe bimetallic nanoparticles photocatalyst is compared to various Zn-based bimetallic nanoparticles employed for the removal of industrial dyes and the results are demonstrated in Table-1.

Conclusion

In summary, the ZnO-Fe_2O_3 bimetallic nanoparticles as photocatalyst was synthesized using microwave irradiation method, for the effective photodegradation of brilliant blue and Amaranth dyes. The degradation rates were varied with the NaOH solution concentrations and catalyst amounts. The pseudo-first-order kinetic rates for the decay of both dyes at room temperature were

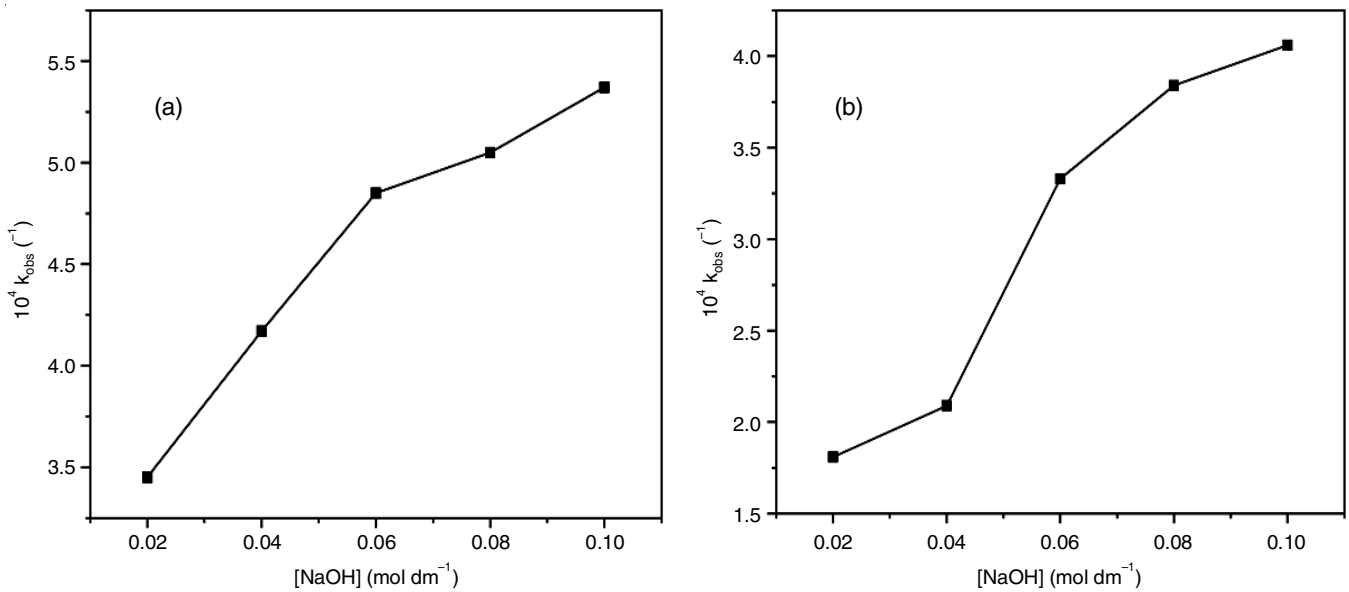

Fig. 7. Plots of rate constant *versus* varying concentrations of NaOH for brilliant blue (a) and Amaranth (b)

TABLE-1
A COMPARATIVE DATA FOR DIFFERENT Zn-BASED BIMETALLIC NANOPARTICLES EMPLOYED IN REMOVAL OF INDUSTRIAL DYES

Photocatalyst	Model dye	Reaction time (min)	Degradation rate (%)	Ref.
ZnO/CdO	Methylene blue	360	97.8	[24]
$ZnOSnO_2$	Methylene blue	150	88.0	[25]
Ag-Zn	Methyl red	60	855	[26]
	Phenol red	60	93.0	
	Eosin yellow	60	78.0	
Zn-Cu	Reactive blue 99	120	98.33	[27]
rGO@$AgZnCo_2O_4$	Methylene blue	105	75.3	[28]
Ag/ZnO	Basic violet 3	30	79.0	[29]
ZnO/CuO NPs/CSC	Reactive red 195	120	80.5	[30]
Ni-ZnO	Methylene blue	270	100.0	[31]
Ag/ZnO	Methylene blue	200	82.6	[32]
Ag@ZnO	Rhodamine B	120	90.0	[33]
Ag/ZnO	Methylene violet	120	88.93	[34]
GO/ZnO	Methylene blue	90	84.0	[35]
ZnSe	Methyl orange	120	75.0	[36]
Cu/ZnSe	Methyl orange	120	87.0	[37]
$ZnCo_2O_4$	Crystal violet	180	84.3	[38]
	Methylene blue		87.9	
	Rhodamine b		89.5	
Zn-Fe BN	Brilliant blue	45	98.0	Present study
	Amaranth	75	93.0	

observed at their respective wavelength. Under the identical conditions, except for the varying presence of [NaOH], the oxidation rate of both dyes was estimated.

ACKNOWLEDGEMENTS

The authors acknowledge the Department of Chemistry, UIS, Chandigarh University for providing essential support to conduct the research work.

CONFLICT OF INTEREST

The authors declare that there is no conflict of interests regarding the publication of this article.

REFERENCES

1. V. Jacometti, *Laws*, **8**, 27 (2019); https://doi.org/10.3390/laws8040027
2. T. Hussain and A. Wahab, *J. Cleaner Prod.*, **198**, 806 (2018); https://doi.org/10.1016/j.jclepro.2018.07.051
3. K. Sathya, K. Nagarajan, G.C.G. Malar, S. Rajalakshmi and P.R. Lakshmi, *Appl. Water Sci.*, **12**, 70 (2022); https://doi.org/10.1007/s13201-022-01594-7
4. S. Varjani, P. Rakholiya, H.Y. Ng, S. You and J.A. Teixeira, *Bioresour. Technol.*, **314**, 123728 (2020); https://doi.org/10.1016/j.biortech.2020.123728
5. S. Sarkar, A. Banerjee, U. Halder, R. Biswas and R. Bandopadhyay, *Water Conserv. Sci. Eng.*, **2**, 121 (2017); https://doi.org/10.1007/s41101-017-0031-5
6. J.J. Soriano, J. Mathieu-Denoncourt, G. Norman, S.R. de Solla and V.S. Langlois, *Environ. Sci. Pollut. Res. Int.*, **21**, 3582 (2014); https://doi.org/10.1007/s11356-013-2323-4
7. B. Lellis, C.Z. Fávaro-Polonio, J.A. Pamphile and J.C. Polonio, *Biotechnol. Res. Innov.*, **3**, 275 (2019); https://doi.org/10.1016/j.biori.2019.09.001
8. S. Benkhaya, S.M. M'rabet and A. El Harfi, *Heliyon*, **6**, e03271 (2020); https://doi.org/10.1016/j.heliyon.2020.e03271
9. R. Sasikala, K. Karthikeyan, D. Easwaramoorthy, I.M. Bilal and S.K. Rani, *Environ. Nanotechnol. Monit. Manag.*, **6**, 45 (2016); https://doi.org/10.1016/j.enmm.2016.07.001
10. P. Singh, M.C. Vishnu, K.K. Sharma, R. Singh, S. Madhav, D. Tiwary and P.K. Mishra, *Desalination Water Treat.*, **57**, 20552 (2016); https://doi.org/10.1080/19443994.2015.1108871
11. G. Mamba, X.Y. Mbianda and A.K. Mishra, *J. Environ. Sci. (China)*, **33**, 219 (2015); https://doi.org/10.1016/j.jes.2014.06.052
12. S. Agrahari, A.K. Singh, R.K. Gautam and I. Tiwari, *Environ. Sci. Pollut. Res. Int.*, **30**, 124866 (2022); https://doi.org/10.1007/s11356-022-23660-y
13. Z. Shen, G. Peng, J. Shi and G. Ya, *Environ. Sci. Pollut. Res. Int.*, **28**, 51786 (2021); https://doi.org/10.1007/s11356-021-14372-w
14. Z. Shen, G. Peng, Y. Gao and J. Shi, *Environ. Sci. Water Res. Technol.*, **7**, 1078 (2021); https://doi.org/10.1039/D1EW00028D
15. B. Pal and M. Sharon, *Mater. Chem. Phys.*, **76**, 82 (2002); https://doi.org/10.1016/S0254-0584(01)00514-4
16. S. Sakthivel, B. Neppolian, M.V. Shankar, B. Arabindoo, M. Palanichamy and V. Murugesan, *Sol. Energy Mater. Sol. Cells*, **77**, 65 (2003); https://doi.org/10.1016/S0927-0248(02)00255-6
17. A. Di Mauro, M.E. Fragala, V. Privitera and G. Impellizzeri, *Mater. Sci. Semicond. Process.*, **69**, 44 (2017); https://doi.org/10.1016/j.mssp.2017.03.029
18. L. Xiang and X. Zhao, *Nanomater.*, **7**, 310 (2017); https://doi.org/10.3390/nano7100310
19. C.B. Ong, L.Y. Ng and A.W. Mohammad, *Renew. Sustain. Energy Rev.*, **81**, 536 (2018); https://doi.org/10.1016/j.rser.2017.08.020
20. R. Peña-Garcia, Y. Guerra, R. Milani, D.M. Oliveira, A.R. Rodrigues and E. Padrón-Hernández, *J. Magn. Magn. Mater.*, **498**, 166085 (2020); https://doi.org/10.1016/j.jmmm.2019.166085
21. K. Raees, M.S. Ansari and M.Z.A. Rafiquee, *J. Nanostructure Chem.*, **9**, 175 (2019); https://doi.org/10.1007/s40097-019-0308-7
22. J. Saha and J. Podder, *J. Bangladesh Acad. Sci.*, **35**, 203 (1970); https://doi.org/10.3329/jbas.v35i2.9426
23. U.G. Akpan and B.H. Hameed, *J. Hazard. Mater.*, **170**, 520 (2009); https://doi.org/10.1016/j.jhazmat.2009.05.039
24. R. Saravanan, H. Shankar, T. Prakash, V. Narayanan and A. Stephen, *Mater. Chem. Phys.*, **125**, 277 (2011); https://doi.org/10.1016/j.matchemphys.2010.09.030
25. L.M. Mahlaule-Glory, S. Mathobela and N.C. Hintsho-Mbita, *Catalysts*, **12**, 334 (2022); https://doi.org/10.3390/catal12030334
26. D.S. Idris, A. Roy, A. Subramanian, S. Alghamdi, K. Chidamabaram and N. Qusty, *J. Inorg. Organomet. Polym.*, **34**, 1908 (2024); https://doi.org/10.1007/s10904-023-02936-x
27. B. Maleki, A.G. Abdulhasan, T.H. Khlaif and M. Mansouri, *Int. J. Environ. Anal. Chem.*, **487**, 1 (2024); https://doi.org/10.1080/03067319.2024.2337222
28. H.M. Abo-Dief, S.M. El-Bahy, O.K. Hussein, Z.M. El-Bahy, M. Shahid and I. Shakir, *J. Alloys Compd.*, **913**, 165164 (2022); https://doi.org/10.1016/j.jallcom.2022.165164
29. M. Sorbiun, E. Shayegan Mehr, A. Ramazani and S. Taghavi Fardood, *J. Mater. Sci. Mater. Electron.*, **29**, 2806 (2018); https://doi.org/10.1007/s10854-017-8209-3
30. M.S. Hasanin, A.H. Hashem, A.A. Al-Askar, J. Haponiuk and E. Saied, *Electron. J. Biotechnol.*, **65**, 45 (2023); https://doi.org/10.1016/j.ejbt.2023.05.001
31. B. Bhushan, K. Jahan, V. Verma, B.S. Murty and K. Mondal, *Mater. Chem. Phys.*, **253**, 123394 (2020); https://doi.org/10.1016/j.matchemphys.2020.123394
32. M.F. Abdel Messih, M.A. Ahmed, A. Soltan and S.S. Anis, *J. Phys. Chem. Solids*, **135**, 109086 (2019); https://doi.org/10.1016/j.jpcs.2019.109086
33. M. Saeed, M. Siddique, M. Ibrahim, N. Akram, M. Usman, M.A. Aleem and A. Baig, *Environ. Prog. Sustain. Energy*, **39**, 13408 (2020); https://doi.org/10.1002/ep.13408
34. M. Afzal, M. Javed, S. Aroob, T. Javed, M. M. Alnoman, W. Alelwani, I. Bibi, M. Sharif, M. Saleem, M. Rizwan, A. Raheel, I. Maseeh, S. Carabineiro and M. Taj, *Nanomater.*, **13**, 2079 (2023); https://doi.org/10.3390/nano13142079
35. N.A.F. Al-Rawashdeh, O. Allabadi and M.T. Aljarrah, *ACS Omega*, **5**, 28046 (2020); https://doi.org/10.1021/acsomega.0c03608
36. V. Beena, S.L. Rayar, S. Ajitha, A. Ahmad, M.D. Albaqami, F.A.A. Alsabar and M. Sillanpää, *Water*, **13**, 2189 (2021); https://doi.org/10.3390/w13162189
37. V. Beena, S.L. Rayar, S. Ajitha, A. Ahmad, F.J. Iftikhar, K.M. Abualnaja, T.S. Alomar, M. Ouladsmne and S. Ali, *Water*, **13**, 2561 (2021); https://doi.org/10.3390/w13182561
38. N. Kitchamsetti, D. Narsimulu, A. Chinthakuntla, C. Shilpa Chakra and A.L.F. de Barros, *Inorg. Chem. Commun.*, **144**, 109946 (2022); https://doi.org/10.1016/j.inoche.2022.109946